

## Supporting Information

### Novel manganese and polyester dendrimer-based theranostic nanoparticles for MRI and therapy of breast cancer

Xiaoxuan Zhou,<sup>‡a</sup> Xiaodan Xu,<sup>‡b</sup> Qihui Hu,<sup>‡a</sup> Yan Wu,<sup>a</sup> Feidan Yu,<sup>a</sup> Chengbin He,<sup>a</sup> Yue Qian,<sup>a</sup>

Yuxin Han,<sup>\*a</sup> Jianbin Tang,<sup>\*b</sup> and Hongjie Hu<sup>\*a</sup>

<sup>a</sup>Department of Radiology, Sir Run Run Shaw Hospital of School of Medicine, Zhejiang University, Hangzhou, Zhejiang, 310027, China. E-mail:

[orangutan@zju.edu.cn](mailto:orangutan@zju.edu.cn); [hongjiehu@zju.edu.cn](mailto:hongjiehu@zju.edu.cn)

<sup>b</sup>Key Laboratory of Smart Biomaterials of Zhejiang Province, ZJU-Hangzhou Global Scientific and Technological Innovation Center, and College of Chemical and Biological Engineering, Zhejiang University, Hangzhou, Zhejiang, 310027, China., Zhejiang University, Hangzhou, Zhejiang, 310027, China. E-mail: [jianbin@zju.edu.cn](mailto:jianbin@zju.edu.cn)

<sup>‡</sup>The authors contributed equally to this work.

#### Supporting data

**Table S1.** Key parameters of MHD samples. Detailed hydrodynamic diameter, zeta potential, and longitudinal relaxivity ( $r_1$ ) were provided.

G1-Cys /mg	MnCl <sub>2</sub> /mg	Hypericin /mg	H <sub>2</sub> O /mL	Hydrodynamic diameter/nm	Zeta potential/mV	$r_1$ relaxivity
50	2.5	0.04	5.0	58	-7.7	3.3
50	5	0.04	5.0	91	-7.2	5.8
50	5	0.08	5.0	130	-7.6	6.1
50	5	0.02	5.0	90	-7.5	5.7
50	10	0.04	5.0	289	-7.8	6.5

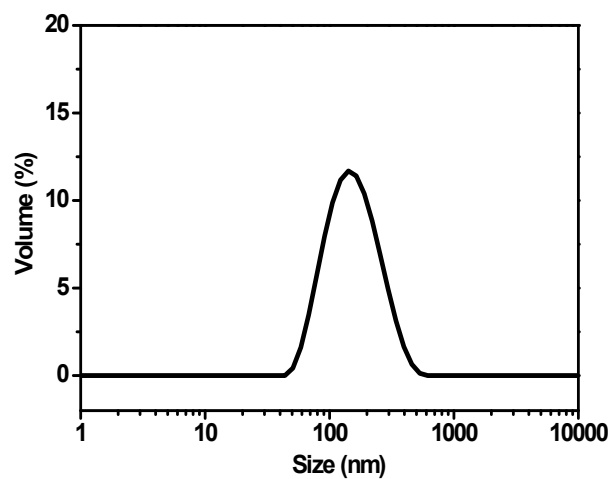


Figure S1. The hydrodynamic size of MD.

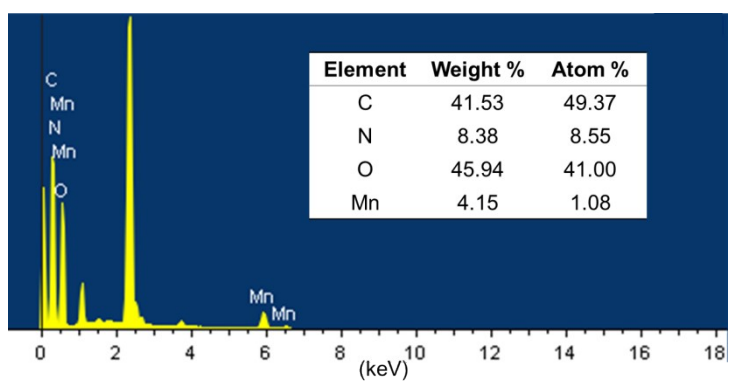


Figure S2. The EDS spectrum and elements data of MHD.

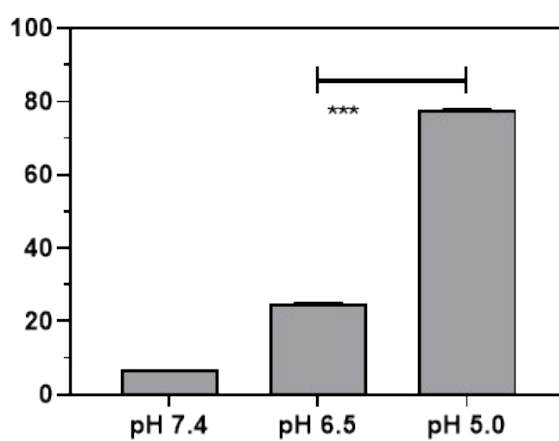


Figure S3. Mn release profiles from MHD ( $0.5 \text{ mg mL}^{-1}$ ) in different pH conditions after 24 h.

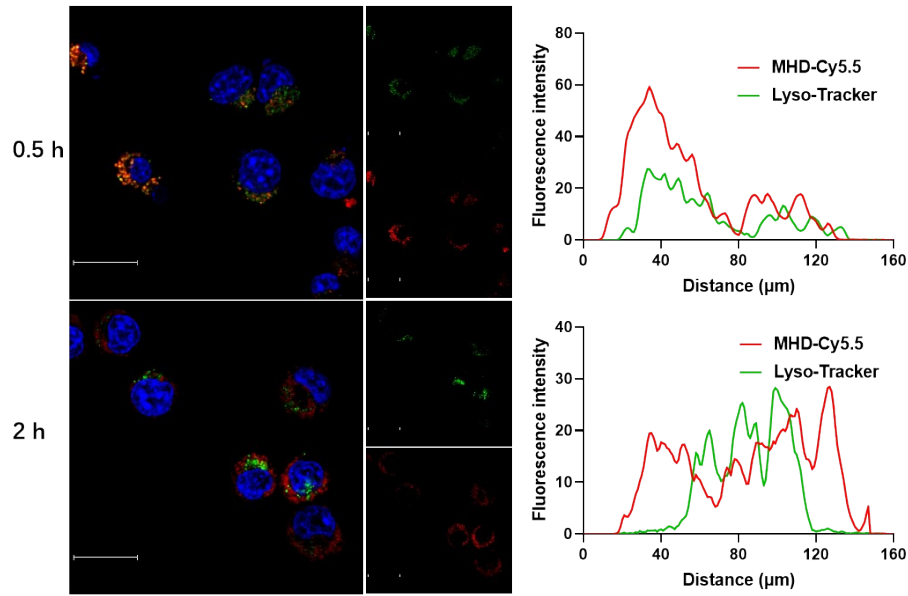


Figure S4. Colocalization and quantitative analysis of MHD-Cy5.5 with lysosomes in 4T1 cells for 0.5 h and 2 h. 4T1 cells were stained for lysosome (LysoTracker, green), nuclei (Hoechst 33342, blue), and detected by CLSM (Scale bar = 20 μm).

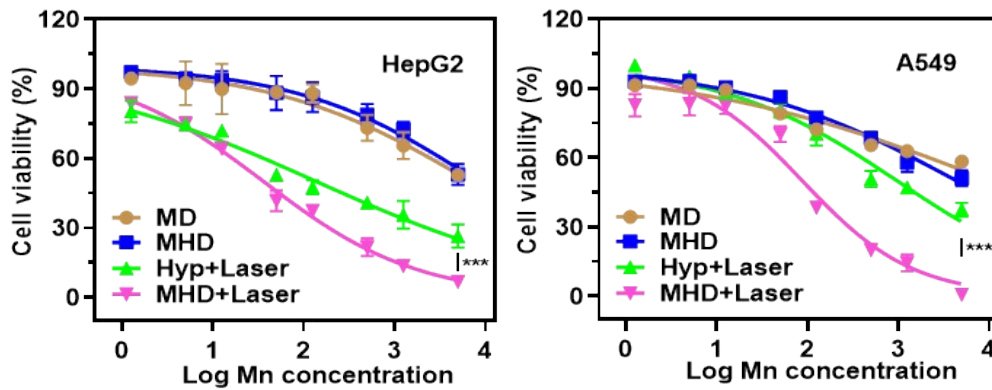


Figure S5. Cell viabilities of A549 and HepG2 cells treated with increased concentrations of MD, free hypericin with laser irradiation (Hyp+Laser), and MHD with or without laser irradiation (MHD+Laser).

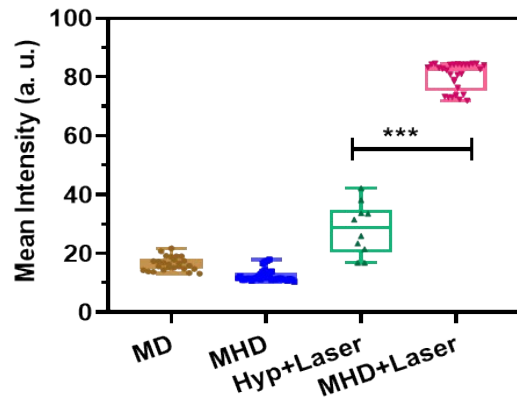


Figure S6. Confocal images of the ROS mean intensity by imageJ by five groups treatment.

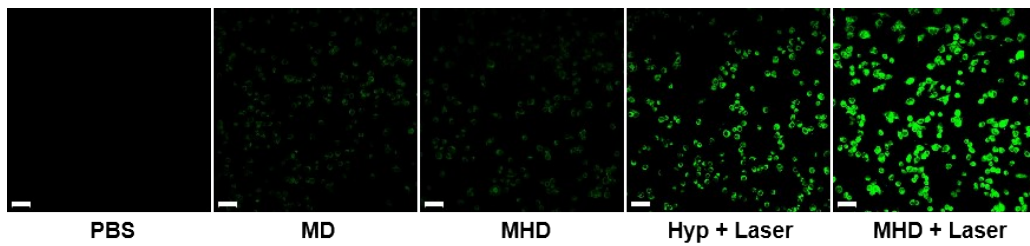


Figure S7. Flow cytometry analysis (b) and confocal images (c) of toxic hydroxyl radicals from endogenous  $H_2O_2$  after different treatments (Scale bar = 50  $\mu m$ ).

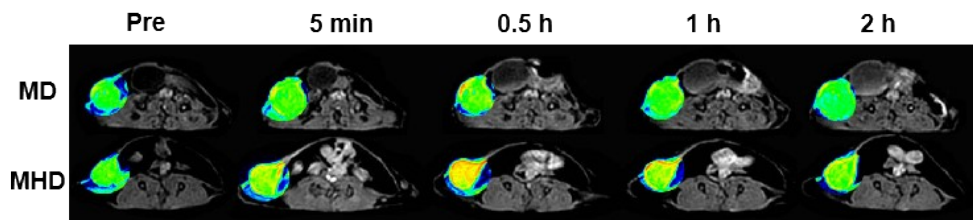


Figure S8. The pseudo-color MRI images of the 4T1 tumor-bearing mice before and after MHD or MD injection ( $0.1 \text{ mmol Kg}^{-1} \text{ Mn}$ ).

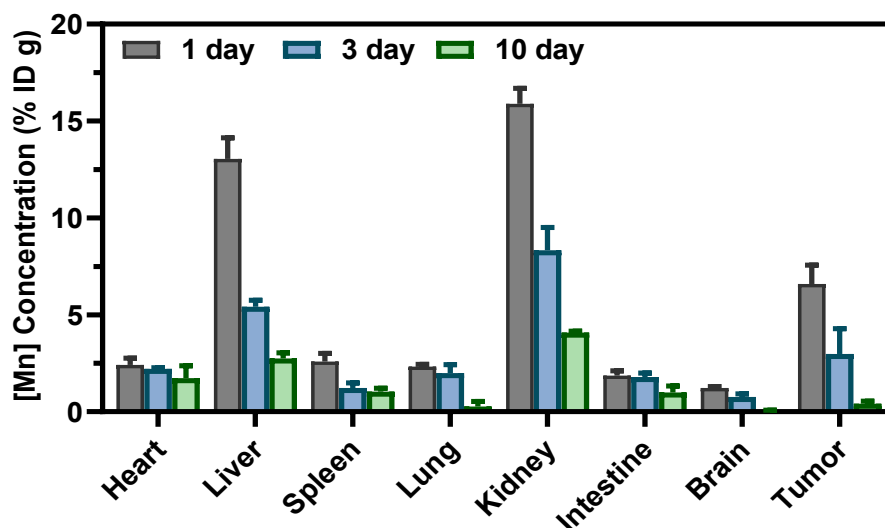


Figure S9. Biodistribution of MHD by measuring Mn concentrations on days 1,3 and 10 after intravenous injection.

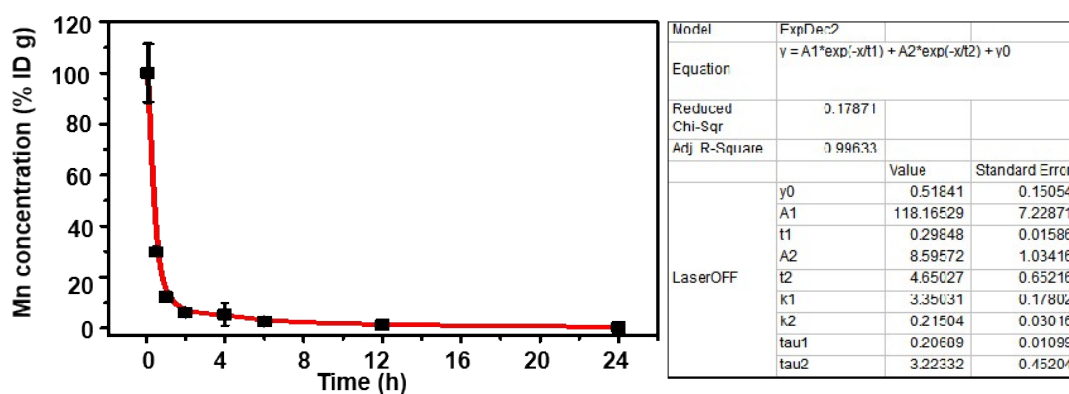


Figure S10. The blood circulation of MHD *via* Mn concentration measurement for 24 h after intravenous injection. Data are presented as mean  $\pm$  SD (n = 3)

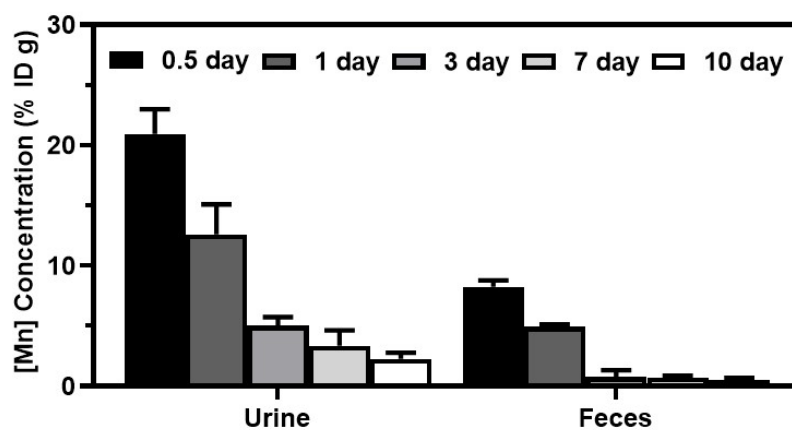


Figure S11. Excretion behaviors of MHD in the mice bearing 4T1 tumors after intravenous injection dosage of  $0.1 \text{ mmol Kg}^{-1} \text{ Mn}$ .

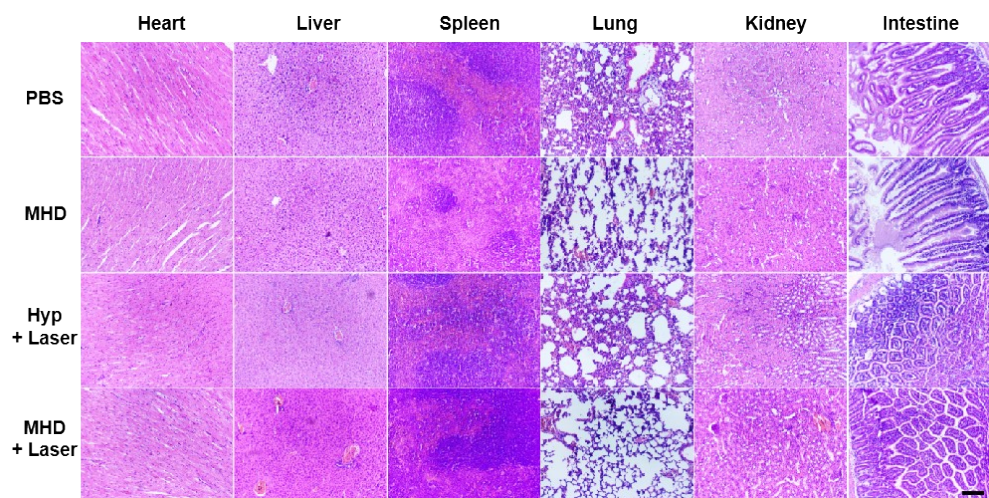


Figure S12. H&E-stained images of the major organs from four treatment groups (PBS, MHD, free hypericin with PDT, and MHD with PDT) mice after 18 days (hypericin  $10 \mu\text{g Kg}^{-1}$ ,  $0.1 \text{ mmol kg}^{-1} \text{ Mn}$ ,  $595 \text{ nm}$ ,  $2.5 \text{ mW cm}^{-2}$ ). Scale bar:  $100 \mu\text{m}$ .